Journal of Geophysical Research: Oceans

RESEARCH ARTICLE
10.1002/2018JC013778

Special Section:
Sea State and Boundary Layer Physics of the Emerging Arctic Ocean

Low-Level Baroclinic Jets Over the New Arctic Ocean

Peter Guest[1], P. Ola G. Persson[2], Shouping Wang[3], Mary Jordan[1], Yi Jin[3], Byron Blomquist[4], and Christopher Fairall[5]

[1]Naval Postgraduate School, Department of Meteorology, Monterey, California, USA, [2]Cooperative Institute for Research in Environmental Studies, University of Colorado, Boulder, Colorado, USA, [3]Naval Research Laboratory, Monterey, California, USA, [4]University of Colorado at Boulder, Boulder, Colorado, USA, [5]National Oceanic and Atmospheric Administration Earth System Research Laboratory, Boulder, Colorado, USA

Key Points:
- Low-level baroclinic jets in the Arctic are common during cold seasons in ice edge regions due to the horizontal contrast in surface temperature and turbulent heat fluxes
- During the Sea State cruise all five of the major (>10 m s^{-1}) surface wind events were associated with atmospheric jets that had cores near the top of the boundary layer
- With enough resolution and proper representation of surface conditions, numerical models are able to simulate the jets with good skill

Correspondence to:
P. Guest,
pguest@nps.edu

Citation:
Guest, P., Persson, P. O. G., Wang, S., Jordan, M., Jin, Y., Blomquist, B., & Fairall, C. (2018). Low-level baroclinic jets over the new Arctic Ocean. *Journal of Geophysical Research: Oceans*, *123*, 4074–4091. https://doi.org/10.1002/2018JC013778

Received 11 JAN 2018
Accepted 25 MAR 2018
Accepted article online 3 APR 2018
Published online 28 JUN 2018

Abstract During the Sea State cruise in the fall of 2015, in the Chukchi/Beaufort Sea region, there were five strong (>10 m s^{-1}) surface wind events associated with low-level atmospheric jets. These jets were analyzed using rawinsonde observations, ship measurements, and a numerical forecast model. The jets occurred when easterly winds aligned with the ice edge, generating low-level baroclinicity in a direction favorable for increasing the geostrophic wind speed toward the surface. The maximum wind speed usually occurred at the top of the atmospheric boundary layer with wind speeds greater than 8 m s^{-1} extending through the capping inversion to 2,000–3,000 m elevation, with winds decreasing toward the surface in the boundary layer due to friction. The width (crosswind) dimensions of the jets were 250–400 km and they existed downwind for as long as the winds remained generally parallel to the ice edges, typically several hundred kilometers. Thermal winds calculated from crosswind-oriented rawinsonde temperature profiles matched the observed vertical wind speed gradients in the inversion regions, indicating that the jets were in quasi-geostrophic (inversion layer) or quasi-frictional (boundary layer) balance, with low Rossby numbers. We define these as "baroclinic" type jets, which are distinct from "ice/sea breeze" type jets which flow more down the pressure and density gradients, and have high Rossby numbers. The operational model analyses matched the observations quite well, giving confidence that these types of jets can be simulated and predicted as long as the models have sufficient resolution and accurately parameterize vertical heat fluxes.

Plain Language Summary In recent years, the sea ice that covers the Arctic Ocean has been dramatically decreasing. In places such as the Chukchi and Beaufort Seas (which are northwest and north of Alaska, respectively), there are large areas of open water in the fall season, where 20 years ago there was a thick sea ice cover. When cold Arctic air comes in contact with this relatively warm water, the lower part of the atmosphere heats up. This causes the air to become lighter which decreases the air pressure compared to the air over the remaining sea ice area, which is cold and dense. This contrast in temperature and pressure generates high winds near the surface called "jets." During a recent scientific cruise in the Chukchi and Beaufort seas, the authors launched instrumented weather balloons called rawinsondes which measured temperature, humidity, pressure, and wind profiles during several jet events. These wind events had big impacts on the ocean and ice cover by transmitting momentum to the surface, creating waves, circulations in the upper ocean and destruction of sea ice. These jets, and other phenomena usually associated with more open water, may cause wind speed to increase in the future when there is less sea ice. These jets can be predicted by weather forecast models but present a challenge for global climate prediction models because these climate models do not have a fine enough resolution to accurately simulate the jets.

1. Introduction

This is a study of low-level atmospheric jets (LLJs) that were observed in the Chukchi and Beaufort Seas during the fall of 2015. The Office of Naval Research (ONR) sponsored the "Sea State and Boundary Layer Physics of the Emerging Arctic Ocean" program that was focused on understanding physical processes related to ocean surface waves in the Arctic. The central activity of this program was a cruise (hereafter referred to as the "Sea State cruise") performed by the ice breaker *R/V Sikuliaq* in October and early

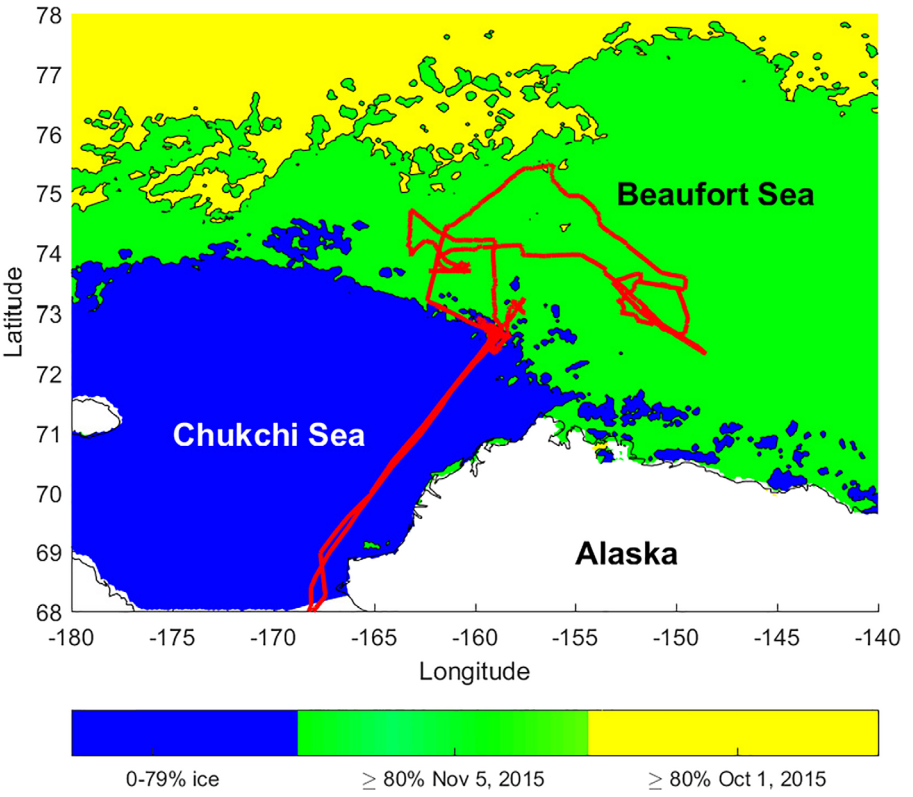

Figure 1. The Sea State cruise track of the *R/V Sikuliaq* (red line) showing AMSR2 ≥ 80% sea ice concentration in the Chukchi and Beaufort Seas on 1 October (yellow) and 5 November (green) and throughout the cruise (blue, 0–79% concentration). Other isopleths such as 50% and 20% are located close to the 80% isopleths. The blue areas were generally ice free during the cruise while ice conditions in the green regions were highly variable in space and time. AMSR2 data courtesy of University of Bremen, https://seaice.uni-bremen.de/sea-ice-concentration/ (Spreen et al., 2008).

November (Figure 1) (Thomson et al., 2018). During this cruise, there were three especially strong wind events near the ice edge that had significant impacts on wave generation, ice deformation, and ice destruction processes, in addition to impacting ship operations. There were two other cases of weaker wind events. Our atmospheric measurements using upper-air (rawinsonde) and shipboard systems revealed that all five of these events were associated with low-level-jets (LLJs), defined as wind features characterized by distinct and significant wind speed maxima in the atmospheric boundary layer (ABL) or capping inversion layers.

Much of the impetus for the Sea State experiment came from the fact that the Arctic, especially the Chukchi and Beaufort Sea regions during the fall, are undergoing dramatic decreases in ice cover. This allows the formation of waves which never existed in this region before and are the central theme of this special *Journal Geophysical Research* issue. Although no significant trend toward increasing wind speeds has yet been detected in the area (Thomson et al., 2016), there are several reasons to expect that the wind stress driving the wave growth is likely to increase in the near future, including (1) a less stable lower atmosphere with deeper ABLs (e.g., Bintanja et al., 2012), (2) the formation of mesoscale cyclones such as polar lows over the open water (e.g., Inoue et al., 2010), (3) changes in synoptic storm tracks (e.g., Wang et al., 2017), and (4) the increase in low-level baroclinicity associated with ice edges and marginal ice zones (MIZs) in regions that previously were entirely ice-covered. This last process is the focus of this paper.

LLJs come in many forms and are common in the Arctic (Jakobson et al., 2013; Walter & Overland, 1991). Tuononen et al. (2015) describe the various types of LLJs and used reanalysis data to create an LLJ climatology, which included the Arctic. They conclude that "the vast majority of LLJs are associated with either sea ice or topography." Inertial oscillation type jets or "nocturnal jets," first described by Blackadar (1957), occur at night when radiational surface cooling stabilizes the atmosphere, which cuts off the frictional contact with the surface of air parcels that were previously in frictional balance. These parcels accelerate as they go down the pressure gradient on their way to geostrophic balance. Using observations over the Weddell Sea

and Baltic Sea, respectively, Andreas et al. (2000) and Vihma and Brümmer (2002) describe advective/synoptic analogies to nocturnal jets. In these cases, synoptic-scale events of well-mixed ABL air, often from the open ocean, is advected over the sea ice, where the surface cooling stabilizes it and decouples the airflow aloft from the surface, thereby removing the surface frictional force. The result is an acceleration, forming a LLJ that undergoes inertial oscillations, similar to a nocturnal jet. Smedman et al. (1993) present a similar warm season case with LLJs forming over the relatively cool Baltic Sea surface due to the advection of warm air and low-level stabilization. Tuononen et al. noted that within ice edge baroclinic zones, more LLJs occurred on the sea ice side compared to the open ocean side suggesting that low-level decoupling and inertial oscillations may be important near ice edges. Warm core cyclonic systems such as polar lows must have LLJs to remain in quasi-geostrophic balance. However, the jets in this paper were not associated with polar lows. LLJs are also formed in gravity flows, such as katabatic winds, and once generated by topography, can extend outward for a few hundred kilometers over a flat surface. Gravity flows are characterized by relatively cold temperature, shallow depth and turning anticyclonically downwind from the source regions once unconstrained by topography (e.g., Renfrew & Anderson, 2006). Topography can generate many other types of jets due to slope, blockage, and gap effects (Tuononen et al., 2015), but we do not have any evidence that topography played a major role during the Sea State cruise.

Baroclinicity (horizontal variations in density) can create LLJs (e.g., Doyle & Warner, 1993; Moritz, 1977; Savijärvi et al., 2005) and is especially relevant in cold season ice edge cases where contrasting surface temperature and heat flux conditions create sharp horizontal gradients in the lower atmosphere (Langland et al., 1989; Persson & Vihma, 2016). Baroclinic LLJs form in "reverse shear flow" situations where the thermal wind vector opposes the geostrophic wind. Polar low genesis is often associated with baroclinic LLJs. For example, Terpstra et al. (2016) found that in reverse shear flow cases, polar lows form to the left (looking downwind) of a baroclinic zone and LLJ associated with the ice edge and sea surface temperature gradients. We define two types of LLJs associated with low-level baroclinicity: the "ice/sea breeze" type and the "baroclinic" type. Both types are related to baroclinicity, but air parcels in the ice/sea breeze type flow predominately down the pressure and temperature gradients and the parcel acceleration is a significant term in the momentum equation. In contrast, baroclinic LLJs, as defined here, are in either geostrophic or frictional balance and the acceleration term is small. The air parcels are flowing at nearly right angles to the pressure and temperature gradients, with some turning toward low pressure in the ABL. Another way to express the difference is that ice/sea breeze type LLJs have large (>1) Rossby numbers, R_o, where R_o is the ratio between inertial and Coriolis forces, while baroclinic types have small (<1) R_o. There is a gray area between the two types ($R_o \sim 1$) and some LLJs may change character in space and/or time from ice/sea breeze types into a baroclinic type. A further distinction can be made concerning baroclinic LLJs. They can be caused by sloping inversions ("Sloping Inversion type") which occur when an inversion or stable layer has horizontal changes in vertical location while below in the ABL and above in the free atmosphere there are relatively negligible horizontal temperature gradients (e.g., Davidson et al., 1992). The other type of baroclinic LLJ is more general and occurs whenever there are horizontal changes in temperature due to changes in air mass temperature ("Air Mass Change type") such as would occur within a differentially surface-heated ABL.

This paper uses the term "ice edge" as if this were some distinct feature. In reality, the ice cover features in the ice edge region or marginal ice zone (MIZ) that we observed were highly complicated, with a variety of convoluted features. We used a satellite-derived 80% ice concentration contour to indicate an "ice edge," but the reader should understand that this is shown only to represent the general orientation of the temperature gradients across the MIZ and give the reader a general sense of the various LLJ orientations with regard to the large-scale surface temperature variations. All times and dates are in the year 2015 and use the Coordinated Universal Time (UTC) convention. The paper is organized as follows: after this introduction, we will describe the measurement, analytical, and numerical analysis methods, followed by a presentation of the observed and modeled results from the cruise and finally a summary and discussion of the key findings and implications.

2. Methods

2.1. Measurements and Accuracy

This paper primarily relies on the wind, humidity, temperature, and pressure measurements from Vaisala RS-92 rawinsondes attached to 100 g weather balloons launched from the fantail of *R/V Sikuliaq*, and similar

measurements collected continuously from the ship at an elevation of 17 m (see Persson et al., 2018). We obtained data from 169 rawinsonde soundings during the cruise, nominally spaced at 6 h intervals which were decreased to 2–3 h during interesting periods, such as the LLJ events described in this paper. Sometimes, we were able to create ascending and descending profiles from one sounding by inserting a plastic syringe into the balloon and creating a small helium leak. This caused the balloon to ascend to a relatively low altitude (such as 5,000 m) and then descend fairly close to the ship a few minutes later.

The claimed total uncertainty of the RS-92 rawinsondes (Vaisala, 2013) for temperature, wind speed, and wind direction are 0.5°C, 0.15 m s^{-1}, and 2°. To verify the temperature accuracies in an experimental setting, we compared lowest level rawinsonde values with the calibrated ship sensors. We also made comparisons between several ascending and descending profiles of the same rawinsonde and found that at all levels the differences were typically 0.2°C to 0.3°C and this included turbulent fluctuations. Biases between different rawinsondes were less than 0.2°C.

The wind vector measurements were affected by many factors and the estimated errors were considerably greater than the Vaisala values stated in the previous paragraph. Due to the swinging rawinsonde below the balloon and turbulence and noise in the GPS signal, radiosonde wind vector calculations are smoothed by the Vaisala software and therefore may not be able to fully resolve the smallest (<200 m) vertical scale wind fluctuations. Also the rawinsonde ascents are only one realization of the turbulent atmosphere and the measured values are not necessarily the mean values for that period due to the natural gustiness of the ABL. We used relatively slow ascent rates (~4 m s^{-1}) to increase the vertical resolution of the GPS-derived wind vector. Comparison of nearby (within 2 km) ascending versus descending portion of the same radiosondes showed that the wind speeds were less than 2 m s^{-1} different 95% of the time and the directions were within 10° of each other at all elevations except at the lowest levels. These are measures of the overall accuracy of the wind measurements representing short-term mean values. The comparison of the ascending (contaminated) and descending (free air) rawinsonde wind data showed that there were often significant ship effects (usually a slowing of the wind speed) up to 50 m and sometimes as high as 120 m elevation. This was especially true during the high wind events (that are the focus of this paper) because the only way the rawinsonde balloons could be launched successfully was to intentionally block the wind at the fantail launch location by orienting the ship bow directly into the wind. No corrections or removal of low-level wind data were performed for the analyses or figures because only a small portion of the atmospheric boundary layer (ABL) was affected; useful comparisons between different profiles were still possible since the blocking effects were similar for the different high wind launches.

2.2. Measurement Strategy

There were no long-range aircraft available for this cruise. Therefore, the measurement challenge was to separate spatial versus temporal variations as observed from sequentially launched rawinsondes from the typically moving *R/V Sikuliaq*. The ideal strategy for quantifying horizontal variations and allow thermal wind calculations would be to perform rawinsonde soundings while the ship moves as fast as possible crosswind to the jet axis and assume quasi-steady state conditions between soundings. However, on a ship with many different scientific measurement goals, this was not usually possible, so the actual strategy was to launch as many radiosondes as possible during interesting events, hoping there will be opportunities for useful cross sectional information. Fortunately, the ship movements did result in several suitable sets of two or more rawinsonde profiles in favorable orientations for quantifying thermal gradients and other horizontal features associated with the LLJs.

2.3. Analytical Analysis

The working hypothesis is that the LLJs observed during the Sea State cruise were created by horizontal temperature gradients in the ABL and/or inversion layers. The vertical variation in geostrophic wind vector in pressure coordinates, $\frac{\partial \mathbf{V_g}}{\partial \mathrm{p}}$, can be expressed using the thermal wind equation

$$\frac{\partial \mathbf{V}_\mathrm{g}}{\partial \mathrm{p}} = -\frac{\mathrm{R}}{\mathrm{fp}}\mathbf{k} \times \nabla_\mathbf{p} \mathrm{T_v} \tag{1}$$

where $\nabla_\mathbf{p} \mathrm{T_v}$ is the virtual temperature gradient along a constant pressure surface, **k** is the unit vertical vector, and f, p, and R are the Coriolis parameter, pressure, and gas constant, respectively. If the geostrophic wind direction is at right angles to the temperature gradient, the thermal wind equation can be simplified

$$\frac{\partial V_g}{\partial p} = -\frac{R}{fp}\frac{\partial T_v}{\partial x} \tag{2}$$

Here V_g is the geostrophic wind speed and $\frac{\partial T_v}{\partial x}$ is the crosswind temperature gradient along a pressure surface. We used a finite difference form of equation (2), based on two crosswind radiosonde profiles, to estimate thermal winds for this study. Geostrophic wind speeds (applicable to the midway point between the soundings) are calculated by picking a level just above the LLJ, which was usually near the top of the inversion, setting the geostrophic wind at that level to the average of the two soundings' true wind speed (assumed to be geostrophic), and integrating the wind speed gradient downward from that level using equation (2).

The data analysis included the calculation of a geostrophic adjustment length scale: the Rossby radius of deformation, L_R. This length scale can be determined using data from a single radiosonde sounding. The ABL/inversion Rossby radius of deformation using a two-layer model is

$$L_R = \frac{\left(gH\frac{\Delta\theta}{\theta_0}\right)^{1/2}}{f} \tag{3}$$

where g is the acceleration of gravity, H is the height of the top of ABL-capping inversion, $\Delta\theta$ is the change in potential temperature across the inversion, and θ_0 is the mean ABL and inversion potential temperature. This L_R is a measure of the distance over which a perturbation in the boundary layer (such as a rapid temperature change due to a change in surface forcing) adjusts to geostrophic flow. Grisogono et al. (1998) observed that thermally driven coastal jets had width scales near L_R. Also, idealized numerical and analytical model simulation studies (e.g., Chao, 1985) with air flow parallel to an abrupt linear change in surface temperature (and heat fluxes) show that the wind field will be affected perpendicular to the linear temperature feature on the scale L_R. We expect ice edge LLJs would similarly scale with L_R, which in the Arctic is O(100 km).

Another scale to consider is a horizontal surface temperature variation scale, L_{SFC}. This could apply to a variety of features such as the width of a marginal ice zone, polynya, ice edge curvature, or lead. When L_R is greater than L_{SFC}, then the effect of the surface features on the large-scale air flow will be "smeared out" by the geostrophic adjustment process, while if L_{SFC} is greater than L_R, the size of the surface feature influences the resulting adjustment.

The Rossby radius of deformation concept can also be applied in the downwind direction. Air parcels that undergo an ageostrophic perturbation such as those that might occur in the upwind portion of the LLJ would be expected to reach a force balance on the scale of L_R. A nondimensional ratio similar in concept to the Rossby number (comparing inertial versus forcing effects) can be derived by dividing L_R by the observed LLJ horizontal scales. Ice/sea breeze type jets have width dimensions and entrance region parcel trajectories that occur on scales less than L_R and have significant parcel accelerations. In contrast, baroclinic LLJs have larger distance scales, are in quasi-geostrophic or quasi-frictional balance and have relatively small parcel acceleration.

We can derive another scale representing the horizontal distance over which the ABL reaches thermal equilibrium with the surface via turbulent heat fluxes. The rate of change of temperature over time following an air parcel in a well-mixed ABL, $\frac{d\theta_{ABL}}{dt}$, with no entrainment is determined by

$$\frac{d\theta_{ABL}}{dt} = \frac{C_H\ U_{ABL}(\theta_{SFC} - \theta_{ABL})}{Z_i} \tag{4}$$

where θ_{SFC} and θ_{ABL} are the ABL potential surface (snow, ice, or open water) and air temperatures, U_{ABL} is the average wind speed in the ABL, Z_i, is the top of the mixed-layer height (usually near the inversion base), and C_H is the surface heat transfer coefficient, here as appropriate for θ_{ABL} and U_{ABL}, instead of surface layer values. The solution for this equation is

$$\theta_{ABL} = \theta_{SFC} + (\theta_{0ABL} - \theta_{SFC})\ \exp\left(-\frac{tC_H\ U_{ABL}}{Z_i}\right) \tag{5}$$

where θ_{0ABL} is the initial θ_{ABL}. Substituting average parcel trajectory distance, x, since the surface temperature change

$$x = t\ U_{ABL} \tag{6}$$

results in

$$\theta_{ABL} = \theta_{SFC} + (\theta_{0ABL} - \theta_{SFC})\ \exp\left(-\frac{xC_H}{Z_i}\right) \tag{7}$$

This shows how we can define a temperature adjustment length scale, L_T

$$L_T = Z_i / C_H \tag{8}$$

which represents the distance over which the boundary layer thermally adjusts to a change in surface temperature in forced convection conditions. For this jet study, L_T is compared to the parcel trajectories to determine if the ABL has adjusted to the contrasting ice and open water surface temperatures. Before this occurs, the temperature gradients in the ABL across the ice edge will continue to strengthen as the air parcels travel downwind along the ice edge, as discussed in section 3.4.5. In the Arctic, L_T is typically several hundred kilometers.

2.4. Numerical Analysis

The data collected by the radiosondes was limited in terms of quantifying the 4 d characteristics of the atmosphere. The radiosondes provided, at best, two-dimensional information. These two dimensions are (1) high resolution vertical and either (2a) time (stationary ship) or (2b) one horizontal direction (pair of soundings). Often, distinguishing whether observed variations in wind vector or temperature between soundings were due to variations in space or time or both was difficult. To address this space versus time variation conundrum, one strategy was to use numerical models to provide complete 4 d information on all relevant variables and help sort out some of the variational uncertainties.

During the Sea State cruise, operational weather forecasts were conducted using the Naval Research Laboratory's Coupled Ocean/Atmosphere Mesoscale Prediction System (COAMPS), which represents both a forecast model and a complete three-dimensional data assimilation system. The forecast model is a finite-difference approximation to the fully compressible and nonhydrostatic equations that govern atmospheric motions (Hodur, 1997). The boundary layer is parameterized using a 1.5 order turbulence closure method (Mellor & Yamada, 1982). Initialization of COAMPS forecasts was performed by the Navy Variational Data Assimilation System (NAVDAS), which assimilates all available observations, including temperature retrievals from Advanced Television Infrared Observation Satellite (TIROS) Operational Vertical Sounder (ATOVS) radiance and wind vectors at different heights using Advanced Very High Resolution Radiometer (AVHRR), Moderate Resolution Imaging Spectroradiometer (MODIS), and Visible Infrared Imaging Radiometer Suite (VIIRS) measurements from polar orbiting satellites (Daley & Barker, 2001). COAMPS provided 48 h forecasts twice daily with a 3 h interval output, initialized at 00:00 UTC and 12:00 UTC. The forecast domain was configured to contain three nested grid meshes (45, 15, and 5 km), which have 157 × 166, 268 × 325, and 496 × 412 grid points, respectively. There were 70 levels in the vertical, of which 42 levels were below 2 km. The outer grid included all of the Arctic and much of the North Pacific Ocean while the inner grids were centered on the cruise area. Lateral boundary conditions for the outermost domain are provided every 3 h by the Navy Global Environmental Model (NAVGEM) forecast fields. The initial ocean state (temperature, salinity, geopotential height, and vector velocity) was generated by combining the first guess fields (from the previous forecast or global model output) with observational analysis using the Navy Coupled Ocean Data Assimilation system (Cummings & Smedstad, 2013), which is the ocean component of NAVDAS (Daley & Barker, 2001). The ocean data analysis makes full use of a wide variety of space-based and in situ ocean observations, including SST from various satellites and ships, satellite altimeter, sea ice concentrations, temperature, and salinity profiles from buoy, Argo and expendable bathythermograph data.

This study used the COAMPS initial analyses or short-term ($\leq$12 h) forecasts. The operational COAMPS performed well during the cruise, as verified by the rawinsonde soundings and discussed in detail later. The cruise rawinsonde data were not assimilated by the model. With this good verification under a variety of conditions, we had confidence that COAMPS was also accurate in regions away from the rawinsonde soundings, and therefore could provide valuable information on jet characteristics that was not possible with the measurements alone.

3. Results

3.1. Cruise Overview

During the Sea State cruise, there were five events of wind speeds greater than 10 m s^{-1} at the ship measurement level of 17 m between 3 October and 5 November (Figure 2). All of these events were caused by LLJs near the ice edge (labeled J1–J5 in Figure 2) with winds in the jet cores at least 5 m s^{-1} greater than winds a few hundred meters above the core. The LLJs occurred during time periods: J1 10–14 October; J2 18–19 October; J3 23–25 October; J4 30–31 October; and J5 1–5 November. J2 had ice breeze characteristics

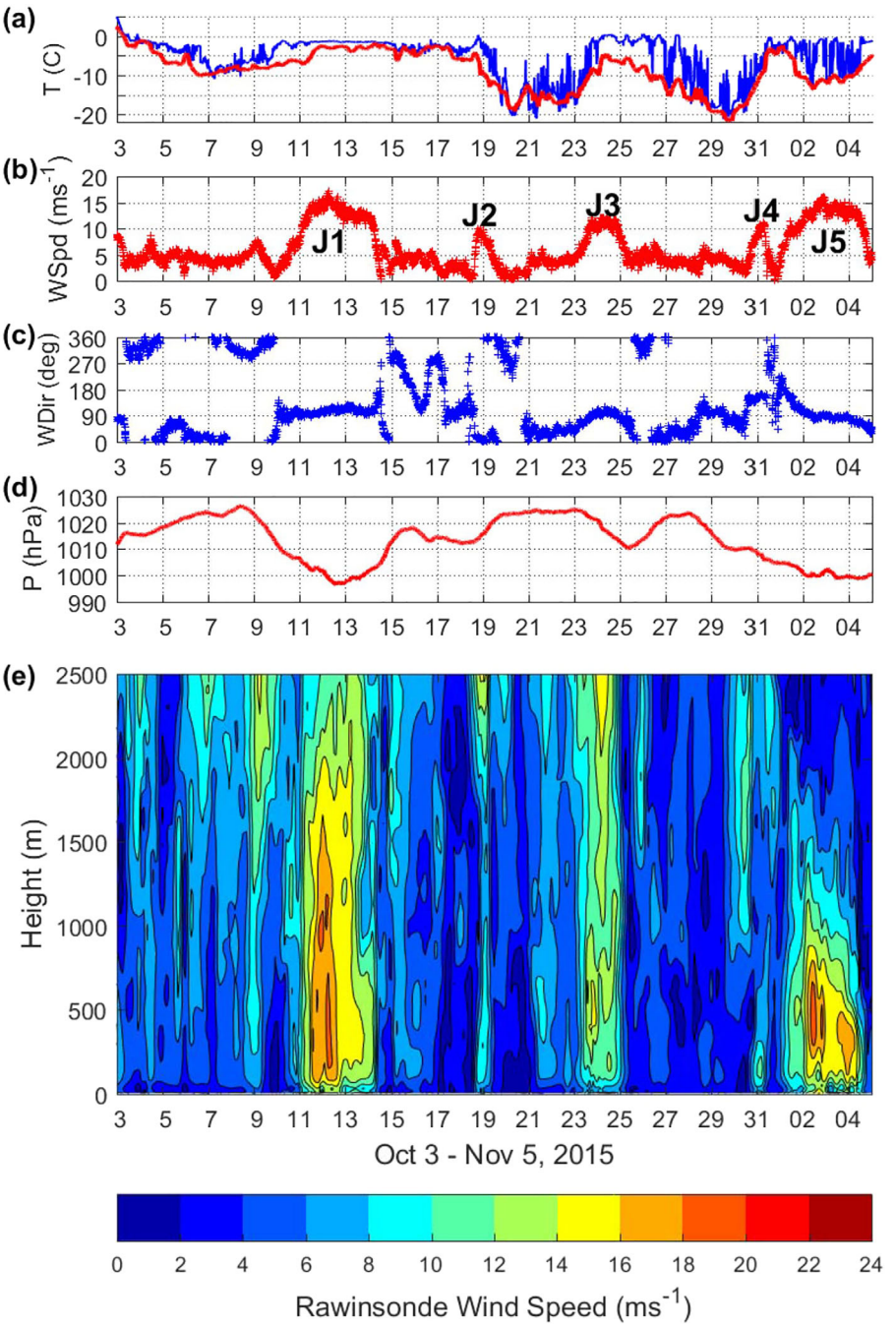

Figure 2. (a) Time series of ship-measured air temperature (red) and infrared-derived surface temperature (blue) for the 3 October to 5 November cruise period. (b) Same for wind speed, with jet events J1–J5 indicated and (c) wind direction (d) surface pressure and (e) time versus height series of 0–2,500 m rawinsonde wind speeds.

with mostly off-ice winds, which underwent large veering between radiosonde measurements, making analysis difficult. J4 was also associated with changing wind direction. Neither of these relatively weaker wind events were well-resolved by the rawinsondes (Figure 2e) and will not be discussed further. On the other hand, the other three events, J1, J3, and J5, represent clearly defined LLJs that were associated with the most significant wind events during the cruise. These jets shared several characteristics: they all lasted for at least 36 h and had periods of at least 24 h when the wind speed and direction were nearly constant. All these cases occurred when the wind directions were easterly or southeasterly, which was parallel to the ice edge (see Figure 1) with the ice on the right looking downwind. This is the type of situation that would be expected to produce baroclinic jets.

Much of the focus of this paper will be on J5, which was the longest-lasting and associated with an almost ideal measurement opportunity: a fast transit across the jet axis as the ship departed the experimental region at the end of the cruise. J1 was a similar case that will be described briefly before presenting the detailed J5 results. Case J3 also involved a transit across the ice edge showing structures similar to those shown for Cases J1 and J5, but will not be discussed further. Other air, ice, and ocean overview measurements associated with all LLJ cases during Sea State are presented by Persson et al. (2018).

3.2. Low-Level Jet J1

On 10 October, an inverted ridge to the north of the ship and a large quasi-stationary low in the Bering Strait region set up a southeasterly flow situation, generally parallel to the ice edge upwind from the ship. The edge of the thin first-year ice at this time and location is fairly represented by the 80% ice concentration isopleth in Figure 3. The edge had numerous protuberances and embayments, leading to local edge orientations that differed significantly from the general larger-scale WNW-ESE orientation. The local ice edge evolved rapidly throughout the 3 day period of jet J1 (see Figure 1 in Smith et al., 2018, and figures in

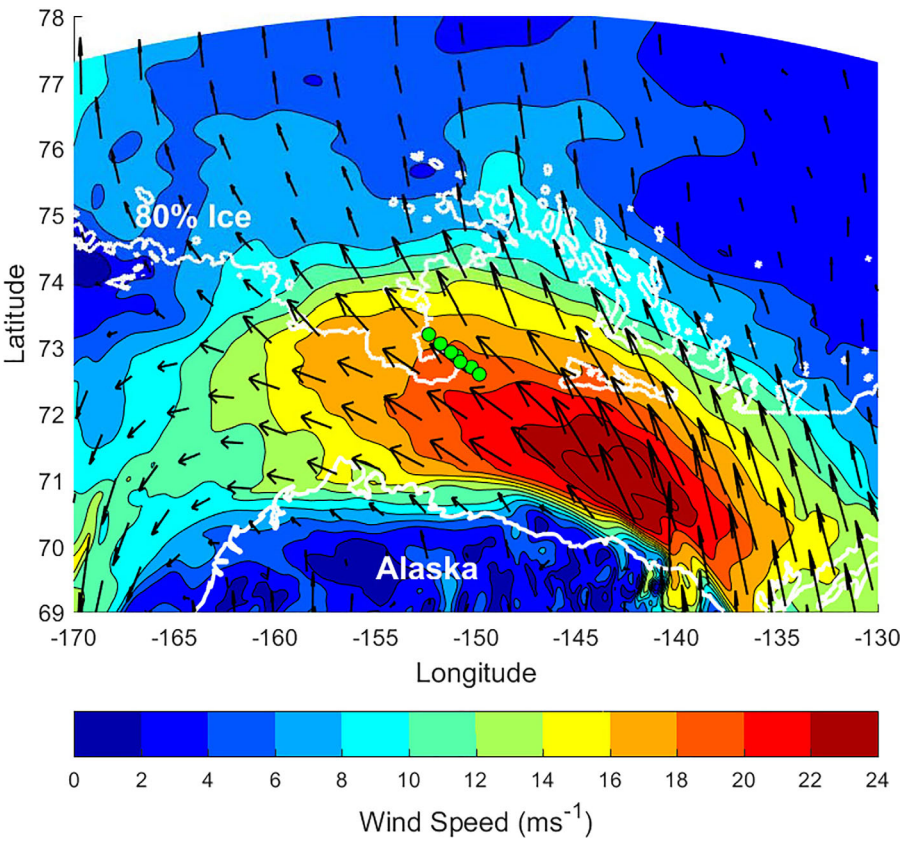

Figure 3. Wind field at 500 m AGL during event J1. Wind speed (m s^{-1}) and downwind direction (arrows) are from COAMPS analysis at 00:00 12 October. The seven rawinsonde launch locations (green dots) for 12 October are indicated. The AMSR2 sea ice edge (white line) for 12 October is represented by the southern edge of 80% sea ice concentration. Wind speed contours are 2 m s^{-1}.

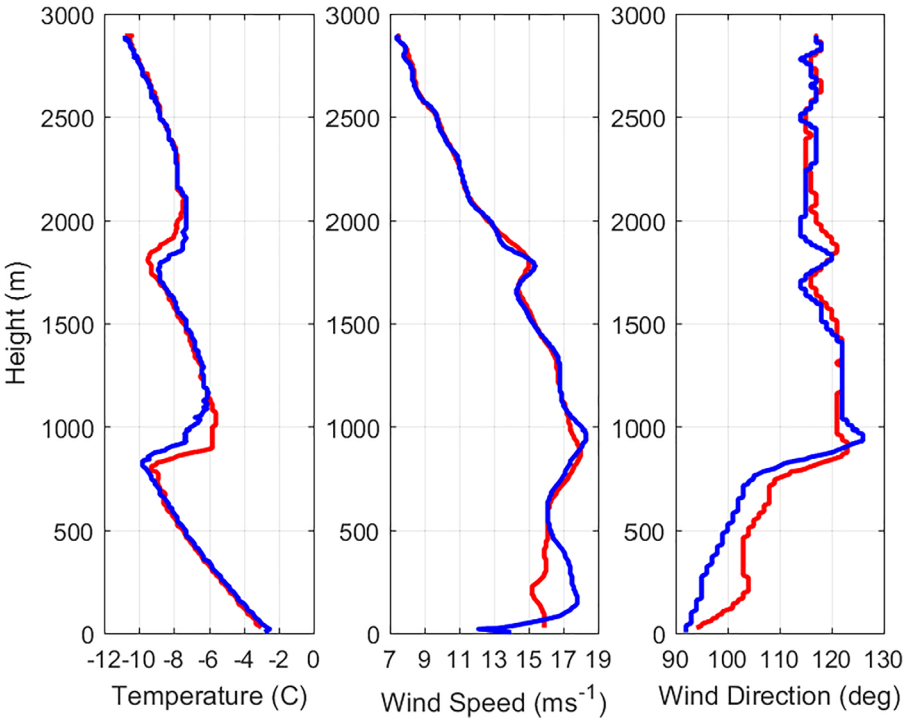

Figure 4. Profiles of air temperature, wind speed, and wind direction from rawinsonde launched 20:59 11 October showing data acquired during the ascending (blue) and descending (red) phases of the rawinsonde flight. Ship location: 72.81N, 150.73W.

Persson et al., 2018, both in this issue, for more detailed ice concentrations near the ice edge at this time, including its evolution). Initially forming to the south of the ship, J1 moved to the north and intensified throughout 10 October reaching a peak wind speed at the ship level of 16 m s^{-1} (Figures 2 and 3). The jet persisted for 3 days until an anticyclone moved into the region from the south on 14 October. Strong winds (>8 m s^{-1}) extended up to 2,500–3,000 m, and for much of the time there was a complicated wind profile with several jet maxima embedded within the overall jet region. J1 had wind flow parallel to the surface temperature gradient and large enough spatial scales to identify it as a baroclinic type jet.

The 20:59 11 October rawinsonde profile had three distinct jet maxima at 200, 1,000, and 1,750 m elevation (Figure 4). We obtained data during both the ascent and descent portions of this 19 min rawinsonde flight. The two higher jet maxima were detected on both flight portions, indicating that these maxima were unlikely to have been caused by random turbulence or wave motion. What is interesting about these maxima is that they are precisely colocated in the most stable parts of the two inversions that are present above the ABL. Although the overall gross characteristics of the jet are clearly baroclinic in nature, the causes of the smaller scale local wind speed maxima are not so clear. Two potential processes may be involved (1) inertial oscillations and/or (2) a "tipping" atmosphere. Inertial oscillation acceleration could occur after the inversion layers are cut off from the surface friction, which could happen in the stable inversion. The second possibility, a tipped inversion layer, could occur through some process creating a large-scale differential vertical velocity, such as a secondary direct circulation. The greatest baroclinicity in these situations would be at the inversion levels, which would generate jet maxima at those levels.

3.3. Low-Level Jet J5

3.3.1. General and Temporal Characteristics

J5 was first detected (>8 m s^{-1} wind) at the ship at 06:00 1 November and lasted until 20:00 4 November, a period of 86 h. Initially, the sea-level pressure (SLP) gradient was produced by a 996 hPa low pressure system approximately 500 km to the SSW just north of the Bering Strait and a strengthening Beaufort High pressure center to the NE of the observing area (see SLP fields in Persson et al., 2018). This caused the geostrophic wind vector to be generally parallel to the SE-NW trending MIZ in the ship region. Once this

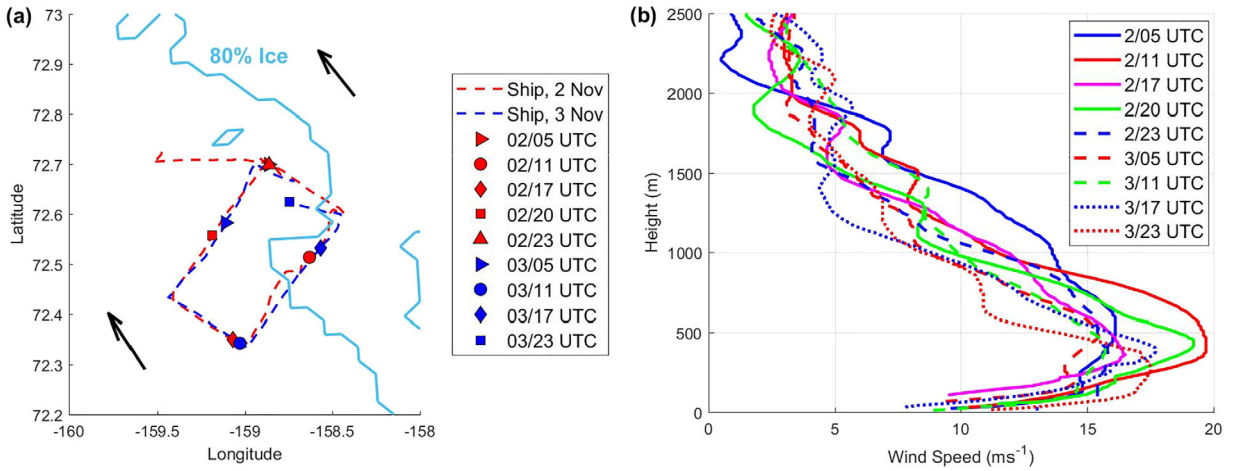

Figure 5. (a) Ship track and location of rawinsondes (symbols) during the J5 period. Arrows show downwind direction at 350 m with a speed of 15.5 m s^{-1} from the 00:00 2 November COAMPS analysis. The 80% ice concentration is from the 2 November AMSR2 product. (b) Corresponding wind speed profiles from these rawinsondes.

direction was established, the wind speed rapidly increased, forming J5. The low remained in about the same location but weakened considerably after the first day and had light core winds, while J5 remained strong and stationary over the ice edge region. The 80% ice concentration isopleth in Figure 5 fairly represents the NW-SE oriented ice edge and suggests that it had some local undulations. These undulations evolved throughout the 4 day period, but in general, the ice edge steadily advanced toward the southwest, encompassing the SW corner of the track rectangle by November 4 (see Figure 25 in Persson et al., 2018, for more detailed concentration fields and the edge evolution). For the earlier part of this period, clouds were present at the top of the ABL but not in the inversion. By 4 November, the inversion had become filled with a thick cloud layer that extended into the ABL.

During most of this period, until 03:00 4 November, the ship was in a "race track" pattern across the ice edge, repeating the same rectangle course (Figure 5a). Radiosonde launches were performed every 3–6 h. During this period, there was a general trend of decreasing height of the J5 wind maximum (Figure 5b). There were no consistent spatial variations detected in the wind speed across the race course pattern. However, the rawinsonde and ship measurements did reveal horizontal variations in temperature at right angles to the wind vector, which provided several opportunities for estimating thermal winds. One example of this is shown later in section 3.4.1; many more cases are described by Price (2016). After 03:00 4 November, the *R/V Sikuliaq* began its final exit from the experimental region, in an orientation almost perpendicular to the wind.

There is good qualitative agreement in the overall duration and height of J5 between the observations and COAMPS analyses. COAMPS resolved the three "pulses" of especially high winds and captured the lower elevation of the core of the final pulse (Figure 6). Wind direction (not shown) was also similarly well-simulated. There were some differences however. The COAMPS core (maximum level) wind speeds are overpredicted by 1–3 m s^{-1}, the predicted onset of J5 was 8 h too early, and the core elevations in the model were about 100 m too low. The model winds in the lowest 100 m are significantly faster than the rawinsonde winds, but in this case this was due to the ship influence described earlier; the model lowest level (10 m) and ship anemometer (17 m) are more accurate (within 2.5 m s^{-1} of each other after correcting for the height difference) than the rawinsonde observations near the surface. It is also possible COAMPS had less friction and mixing in the ABL. COAMPS was used as an operational model with no special postprocessing or tuning; therefore, we can expect that there were errors in initial conditions and surface conditions. Also, the rawinsonde soundings did not match up exactly in space and time with the model output, introducing more uncertainty. Given these challenges, the comparison shows that the model nonetheless performed well at capturing the main wind features of the jet.

The temperature time versus height cross section also reveals good qualitative agreement between COAMPS and the rawinsonde data (Figure 7). A low-level inversion was present in both data sets, with both

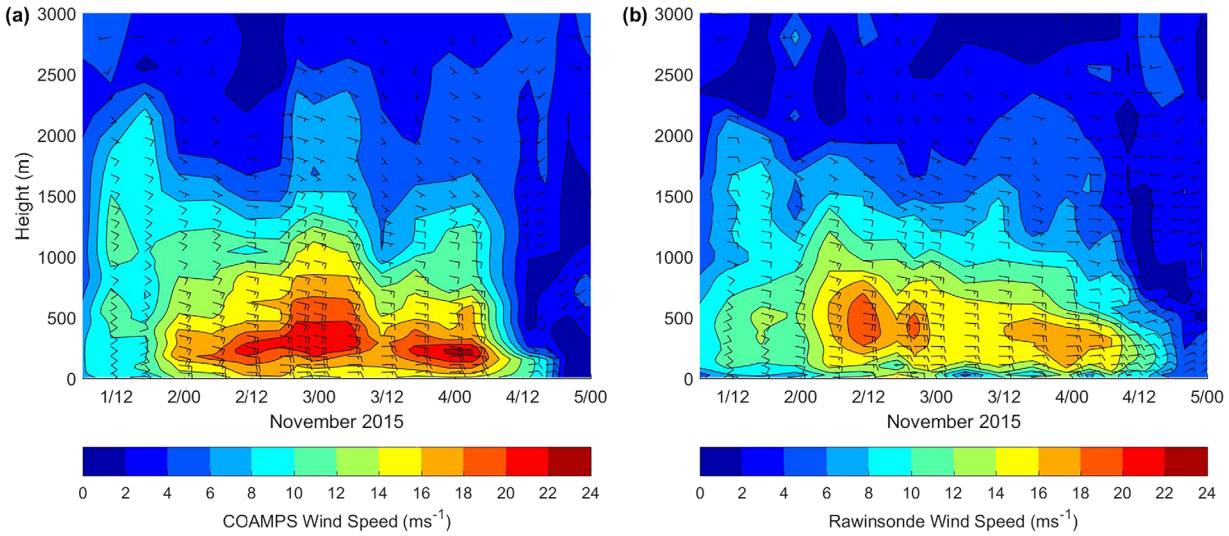

Figure 6. (a) COAMPS wind speed and direction as a function of height and time using the modeled data at the moving location of the radiosonde profiles during the J5 period. (b) Rawinsonde wind measurements for the same period. In both plots, wind barbs use meteorology convention (feathers into the wind, 10 m s^{-1} per full length feather) and North is upward. The contour interval is 2 m s^{-1}.

showing heights for the top of the inversion ranging from around 250 m early in the period to 1,100 m in the central part. Minor differences and the fact that the bottom of the predicted inversion (top of the mixed layer) was too low by about 150 m for much of the period suggests that the magnitudes of some model processes, such as the vertical mixing, are not quite correct. However, this model deficiency does not seem to prevent the LLJ formation, though it may impact details of the LLJ, such as height and magnitude. These comparisons of COAMPS versus rawinsonde data over an extended time period and at different relative positions to the ice edge gave us confidence that the model could be used to quantify spatial and temporal characteristics of J5 that could not be achieved with the radiosonde data alone.

3.3.2. Observed Spatial Characteristics

The exiting of the ship from the experimental region on 4 November provided the opportunity to perform several rawinsonde soundings in a line at right angles to the axis of J5 (Figure 8). For clarity, we show only the AMSR 80% ice concentration line which generally corresponded to the ice edge while the ship was exiting the ice pack at this time. More detailed ice concentration information for this period is contained in

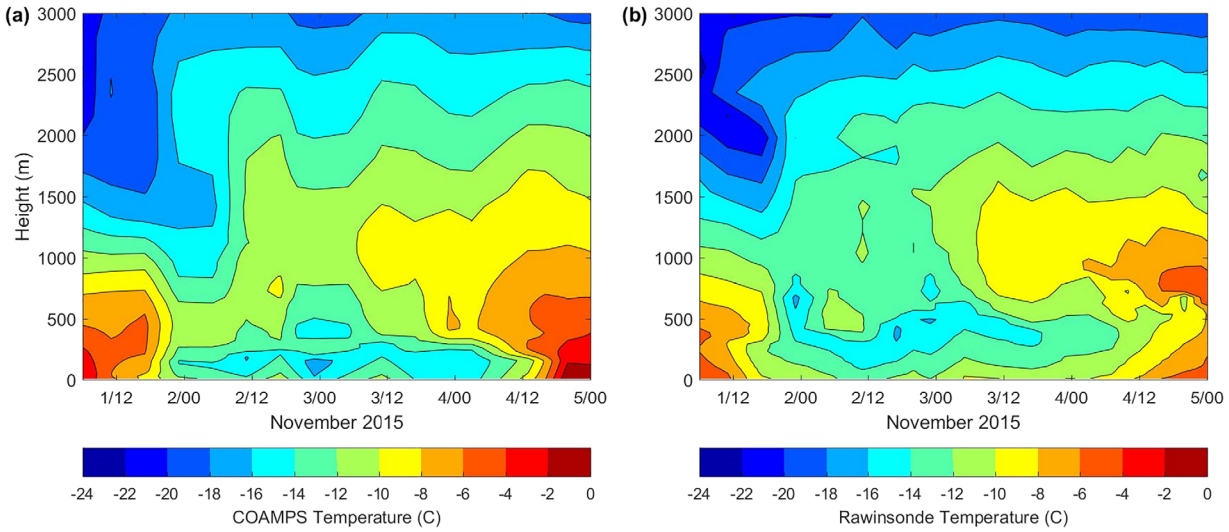

Figure 7. (a) COAMPS temperature as a function of height and time at the moving location of the rawinsonde profiles. (b) Same using rawinsonde measurements. The contour interval is 2°C.

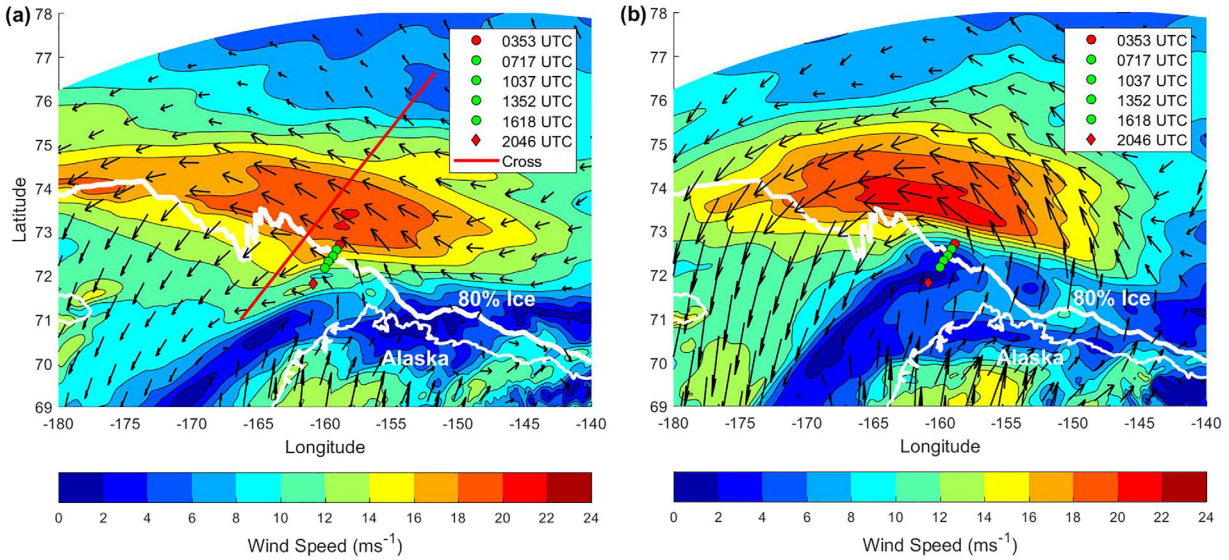

Figure 8. (a) COAMPS 350 m wind fields for 00:00 4 November and (b) 12:00 4 November, showing the location of the radiosondes and 80% AMSR ice concentration contour for 4 November. The red line in Figure 8a indicates the location of the cross section discussed later. The contour interval is 2 m s^{-1}.

Persson et al. (2018). The COAMPS analyses for 00:00 4 November and 12:00 4 November indicate that the jet axis moved to the north by about 100 km between these times, so conditions were not steady state. However, the magnitude and surface footprint of the jet were similar between the two model runs. The distance between the first and last radiosondes on 4 November was 145 km, but using the moving jet location as a frame of reference stretches the "effective" distances since both the ship and jet are moving apart from each other. So in terms of analyzing the jet structure in detail with the radiosondes, the actual 145 km traveled by the ship was effectively 245 km in terms of analyzing the internal structure of J5. This is an example of using the numerical model result to better interpret the observations.

For the first two radiosonde soundings (blue and red colors in Figure 9), a wind speed maximum exists at 350 m elevation with a sharp drop-off from 16 to 8 m s^{-1} at the 600 m level, which marks the top of the jet. Note from the temperature plots of these two soundings (Figure 9) that the jet maxima are at the exact same level as the inversion base, and the top of the jet (where there is a local wind speed minima) is the same as the top of the main inversion (a smaller secondary inversion exists just above). For the rest of the soundings on 4 November, the wind speeds decrease at all levels below 600 m as the ship departs the ice edge region. Interestingly, even as the inversion height grows from 350 to 550 m by the 16:18 4 November

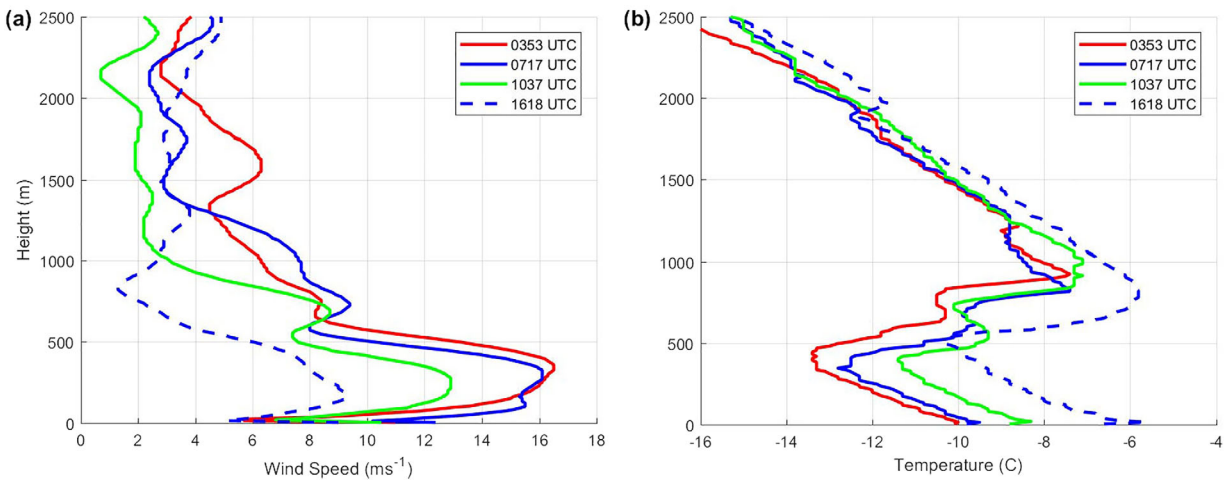

Figure 9. (a) Rawinsonde wind speed and (b) temperature profiles on 4 November.

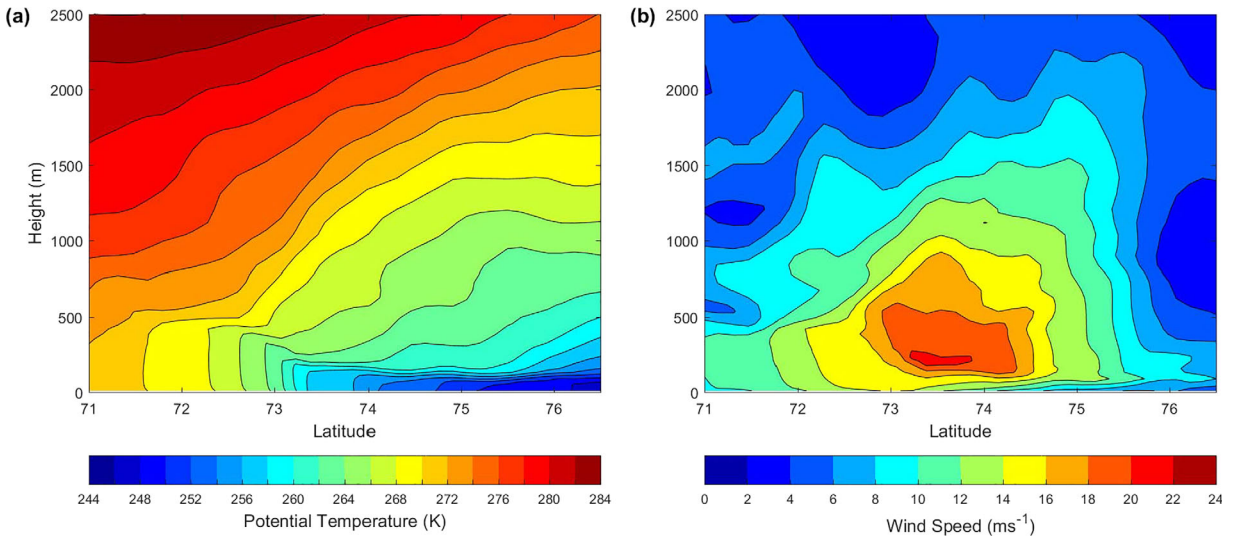

Figure 10. COAMPS space versus height cross sections of J5 for (a) potential temperature (contour interval 2 K) and (b) wind speed (contour interval 2 m s^{-1}) at 00:00 4 November.

sounding, the jet maxima levels decrease, reaching a low of 180 m elevation by the 16:18 4 November sounding. By 20:00 4 November, the ship is no longer in the jet feature (not shown).

3.3.3. Modeled Spatial Characteristics

To understand in more detail the spatial characteristics of J5, we examine the COAMPS distance versus height cross sections of potential temperature (Figure 10a) and wind speed (Figure 10b) at right angles to the wind vector, along the red line indicated in Figure 8a using the 00:00 4 December COAMPS analysis. Similar to the 4 December radiosonde transects, COAMPS shows a rapid decrease in temperature and mixed-layer height from southwest to northeast (left to right in Figures 10a and 10b) associated with the ice edge located at approximately 73°N. This decrease in atmospheric mixed-layer height at the ice edge in the model replicates the structure observed at all ice edges crossings during Sea State (see Persson et al., 2018). There appears to be a dome of cold air located over the ice as indicated by the sloping potential temperature contours above the ABL. The baroclinicity within the ABL and above the inversion both contributed to creating J5. The jet maximum heights were located near the top of the inversion in the COAMPS analysis.

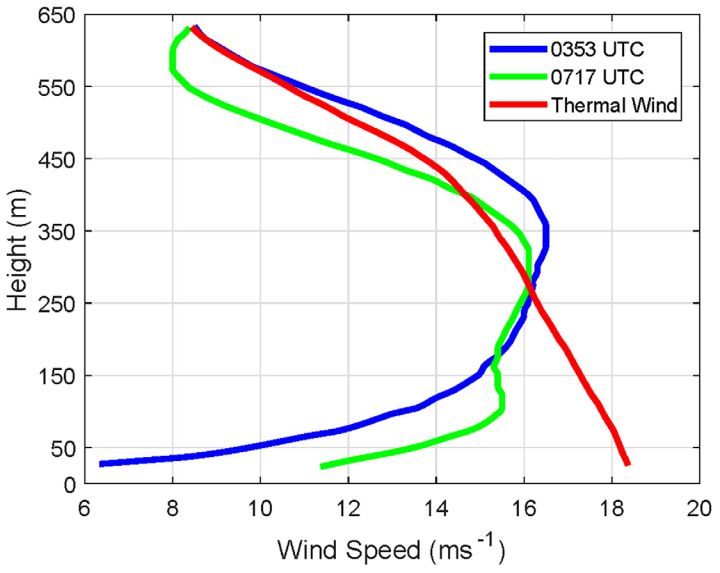

Figure 11. Thermal wind calculation results showing the wind speed from the 03:53 4 November (blue) and 07:17 4 November (green) rawinsonde sounding and the calculated thermal wind based on the horizontal temperature gradient between the two profiles (red).

3.4. Analysis of Results

3.4.1. Rawinsonde (Vertically Derived) Parameters

All the observed and derived parameters used in section 3.4 are rough approximations; the purpose here is to assess J5's basic properties and scaling parameters to determine the significance of various terms in the momentum equation and therefore identify the basic type, i.e., ice breeze versus baroclinic. Using the 03:53 and 07:17 4 November pair of soundings to determine temperature gradients, we apply the thermal wind equation starting at an elevation of 650 m, which is at the top of the jet, assumed to be in geostrophic balance, and also a level where both soundings indicate the same wind speed (8.4 m s^{-1}). From this location to the jet maximum height at 400 m elevation, the geostrophic wind determined from the thermal wind matches the soundings well, falling between the two measured wind speed profiles (Figure 11). Below the jet wind maximum, the geostrophic wind continues to *increase* down to the surface, while the actual winds *decrease* in this region. This is the expected behavior; once in the ABL,

friction slows the wind due to friction even though the pressure gradient is still increasing.

Using the 03:53 4 November sounding (H = 900 m, $\Delta\theta = 11$), the Rossby radius of deformation, L_R was 140 km. The ABL thermal adjustment scale, L_T (using Zi = 425, $C_H = 8 \times 10^{-4}$) was 530 km.

3.4.2. Surface Temperature Length Scales

The obvious maximum horizontal surface temperature variation scale, L_{SFC}, is the width of the MIZ, where increasing ice cover and thickness poleward creates a surface temperature gradient. Based on satellite and cruise measurements (described elsewhere in this issue), this was approximately 200 km. The actual surface temperature variations that we measured varied significantly on a variety of smaller spatial scales; therefore 200 km should be viewed as the upper limit for L_{SFC}, with anything down to a few centimeters (ice floe edges) being a valid length scale for surface temperature variations in the MIZ.

3.4.3. Jet Crosswind Length Scale

The width (crosswind dimension) of the jet, $L_{JW,}$ according to the COAMPS 00:00 4 November analysis was approximately 300 km (Figures 8a and 10b). We can also use the ship data to make an estimate of L_{JW}. During the 4 November ship transit across the jet, surface wind speeds slowed to below 8 m s^{-1} 90 km from the apparent center of the jet (as represented by the 04:00 and 07:00 soundings). But because the jet was moving to the north at about 2/3 of the speed of the ship (see section 3.3.2), a more appropriate scale would be 150 km. Assuming the jet is symmetrical about its axis, this results in a L_{JW} of about 300 km, which is the same as the COAMPS value.

3.4.4. Jet Downwind Length Scale

The J5 jet, as with the other jets modeled by COAMPS during the cruise period, had typical downwind extents of several hundred kilometers, several times greater than the modeled widths. The location of the ship during J5 on the 00:00 4 November model run was about 250 km from where the J5 strong winds initially became strong at the upwind edge of the jet. Defining this location as a perturbation lets us use 250 km as the parcel trajectory scale, L_{JT}.

3.4.5. Interpretation

Several lines of evidence suggest J5 was primarily a "baroclinic" type jet (with low acceleration term) rather than an "ice breeze," "inertial oscillation," or other type of jet. The evidence includes (1) the good match between the thermal wind calculation and the observed wind speed gradients in the inversion above the ABL, (2) the nearly 90° orientation of the wind vector to the temperature gradient, (3) the persistence of J5 (wind speed and direction) in time and space over several inertial periods, (4) the upwind trajectory length L_{JT} (250 km) was longer than the Rossby radius of deformation, L_R (140 km), and (5) the rapid formation once the synoptic forcing aligned the winds with the ice edge. The 4 November rawinsonde pair cases (Figure 11, and in many other cases not shown) used for thermal wind calculations had significant horizontal temperature gradients in both the inversion layer and ABL, although usually they were stronger in the inversion layer. These gradients occurred mostly within the inversion or within the ABL rather than as a result of a sloping inversion.

Below the inversion in the ABL, friction caused the wind speed to decrease and the wind vector was no longer geostrophic. However, the persistence, long trajectory, and apparent good geostrophic balance in the part of the jet in the inversion suggest that in the ABL there is a frictional balance in the momentum equation, with the acceleration term being small compared to the pressure gradient, friction, and Coriolis forces.

Assuming L_R represents the adjustment length scale on one side of an idealized linear perturbation (e.g., the ice edge) the jet width should scale to at least twice that value (or 280 km for J5). The maximum horizontal surface temperature scale L_{SFC} (200 km) was similar, so both the surface forcing and geostrophic adjustment were important factors controlling the jet width. The L_R effects likely extend out from the strong temperature gradient region, so the jet width would be expected to be larger than both scales, but not larger than both combined. The actual observed width of 300 km is consistent with this interpretation.

The ABL thermal adjustment scale L_T (530 km) was considerably longer than the parcel trajectories, $L_{JT,}$ or Rossby radius of deformation, L_R. Also the surface turbulent sensible heat fluxes (driven by air-surface temperature differences) were significant at all locations, but with especially large values over open water (~200–400 W m^{-2}), where the ABL was warmer than over the colder ice (~70–150 W m^{-2}) (see Persson et al., 2018). These two facts indicate that the ABL was not in thermal equilibrium with the surface and the horizontal temperature gradients within the ABL would have continued to strengthen as long as the air parcel trajectories were aligned with the ice edge and the trajectory lengths were not significantly larger than

L_T. This means that, in general, the jet strength will be a function of the distance over which the wind vector is aligned with the edge. If synoptic forcing changes the wind direction or the ice edge curves (on a scale greater than L_R), the jet will dissipate. Individual surface features creating temperature variations on scales less the L_R, such as leads, individual ice floes, smaller scale ice edge meanders, smaller polynyas, and other features are not likely to have a large effect on wind speed variations within an ice edge jet.

In addition to running parallel to the ice edge, J5 was also parallel to the north coast of Alaska, which was 150 km from the ship location. It is possible that the jet was influenced by the coastal topography, but the northern coast of Alaska is quite flat with little orography until the Brooks Range 300 km to the south of the coastline. We could find no evidence of topographic effects extending as far out as J5 or any type of katabatic winds at the coast.

4. Conclusions

4.1. Discussion and Summary

Ice edge jets in cold seasons have undoubtedly been experienced by mariners and captured by numerical forecast and reanalysis products, but there have been very few published reports containing in situ observations of these phenomena. This paper helps alleviate that gap in our knowledge.

The three strongest jets we observed during the Sea State cruise were "baroclinic," as opposed to "ice breeze" types, meaning that the forcing terms in the momentum equation were nearly in balance. The jets and associated baroclinicity were not just ABL phenomena; all of them extended into the capping inversion, and in most cases the top of the jet (where the wind speed no longer decreased with elevation) was colocated with the top of a relatively stable layer (compared to the free atmosphere lapse rate layer above). The ABL baroclinicity was clearly related to the surface temperature and heat fluxes, but the reason for the baroclinicity in the inversion layer was less obvious. The rawinsonde observations and model simulations showed that both J1 and J5 were associated with cold domes over the sea ice regions marked by increasingly thicker and higher inversion tops but with shallower ABLs. The cold domes over the ice shown by the potential temperature can extend hundreds of meters above the inversion top (see Figures 9 and 10 for J5 example). Cold domes over ice are often formed by longwave radiational coupling with lower levels (Overland & Guest, 1991) along with vertical and horizontal advective processes. Persson et al. (2018) suggest that the dome associated with J5 formed due to a series of energy transfer processes including cloud top longwave radiational cooling.

In section 1, it was stated that baroclinic LLJs are caused by either air mass variations or sloping inversions. In all the observed LLJs during the sea state cruise, the horizontal temperature gradients in the ABL and lower part of the inversion layer were similar at all levels, indicative of an air mass change type of baroclinic LLJ. For J5 (and in other cases), the increasing ABL depth toward the open ocean side due to surface heating and entrainment counteracted the geostrophic and LLJ flow (the ABL is colder than the air above) and the bottom of the inversion dipped toward the ice region. Note the inversion was sloping in the opposite direction as would occur in a sloping inversion type LLJ, therefore J5 is an air mass change type of LLJ. Although the base of the inversion layer tipped toward the ice, the top of the inversion and associated stable layers just above are sloped downward toward the open ocean direction; this is the cold dome described in the previous paragraph. This enhances the thermal wind, especially in the upper layers of the inversion. Therefore, the air mass temperatures changed both in the ABL and in the stable layers above; both contributed to the strong jet winds.

The results in this study imply that the synoptic-scale SLP field has a significant impact on the times and locations of these ice edge baroclinic LLJs. In the three cases described here, the center of the Beaufort High was to the northeast of the observation site and over the interior of the pack ice (see Figure 7 in Persson et al., 2018). In the Beaufort Sea region, synoptic evolution as well as the cold dome formation over the ice is biased toward this SLP configuration favorable for ice edge LLJs. Idealized model studies (e.g., Chao, 1985; Guest et al., 1995; Langland et al., 1989) have shown that the water-ice baroclinicity in tandem with an along-ice geostrophic wind is leads to a strong along-ice LLJ, as was observed during Sea State, but that the baroclinicity in the presence of a cross-ice geostrophic wind is still sufficient to develop a weaker LLJ. Further studies with idealized simulations may better quantify the relative roles of synoptic (geostrophic) evolution and pack-ice thermodynamic processes for ice-edge LLJ formation, and its dependence on

features such as the magnitudes of the thermal gradients and baroclinicity, the orientation of the geostrophic flow, and the boundary-layer cloud and mixing processes.

The LLJs described in this paper had many similarities with LLJs that have been associated with polar low genesis. For example, the composite cross sections shown in Terpstra et al. (2016) have slightly larger vertical and horizontal dimensions, but qualitatively compare well with the observational and numerical results in this paper. Our studies focused on the MIZ, while the focus of polar low studies is usually over the open ocean where the deeper ABLs and larger L_R values would be expected to result in larger size baroclinic LLJs. Many of the LLJs associated with reverse shear flow type polar low genesis may originate in the ice edge regions, similar to the Sea State jets, and then advect and become modified over the open ocean.

4.2. Modeling Implications

We introduced the concept of scaling the width of baroclinic jets associated with an ice edge to the Rossby radius of deformation, L_R, associated with the ABL and inversion layer. Obviously this is overly simplistic and many factors affect the jet features. However, we think this is a useful concept in understanding the relative roles of surface forcing and geostrophic adjustment on the overall dimensions of a particular jet.

Successfully modeling these ice edge baroclinic jets requires a grid resolution several times less than L_R. Typically, one would need a grid spacing 6–8 times finer than the scale to be resolved, or $\Delta x = 17–23$ km in this case. The COAMPS inner-grid resolution of 5 km was easily sufficient to resolve the important jet scales. Indeed, the model performed well at characterizing most features in all of the observed jets during the Sea State cruise. We would expect that other regional numerical models would also have success modeling these jets. A crucial factor (besides resolution) is properly parameterizing the surface sensible heat flux and also the radiational coupling between vertical levels, since these are what create the air mass transformation and related ABL and inversion layer thermal gradients that contribute to the jet formation.

In contrast to regional models, global circulation models (GCMs) used for climate change studies, and even some operational global models used for reanalyses, do not currently have sufficient grid spacing to resolve these ice edge jets. Based on the reanalysis studies performed by Tuononen et al. (2015), and anecdotal evidence during the Sea State cruise and other cruises, these low-level baroclinic jets can be a major and even dominant factor in the generation of high wind and wave formation events in MIZ regions during cold seasons. GCMs need to have a way to parameterize the effects of baroclinicly induced wind forcing if they are to accurately capture all the processes affected by surface wind stress.

Properly representing LLJs is crucial in process studies of various air-sea-ice interactions. A common practice while performing numerical studies of sea ice and ocean is to prespecify the atmospheric forcing. However, as we have shown, changes in ice conditions such as a change in the ice edge location create feedbacks to the atmosphere which can then alter the wind pattern by, for example, creating a jet where one did not exist before.

4.3. Significance of Low-Level Baroclinic Jets in the Arctic

These jets can have major impacts on many air-ice-ocean physical processes. All of the major wave events that were the focus of the Sea State cruise were a result of baroclinic LLJs. The wind speed and associated changes in wind stress across a LLJ could generate Ekman pumping, mixed-layer entrainment, and other ocean vertical mixing mechanisms. Wind stress controls ice deformation and can destroy ice by mechanical breakdown or forcing warm ocean waters upward. Enhanced transport of ice can lead to ice advection and deformation, lead formation, and ice streamers (e.g., Hoerton et al., 2014), which can have feedbacks on both atmospheric and the upper ocean processes. Snow transport and aerosol generation are also affected by the strong LLJ winds. The association of some baroclinic LLJs with polar lows can magnify many of these effects.

4.4. The Future Arctic

Strong LLJ wind events in ice edge regions will be of more concern as commercial (tourism and resource extraction), military and scientific activity in the Arctic increases. Strong wind events generated by cyclones and other weather systems will be significantly enhanced if winds line up along an ice edge in the favorable orientation.

If ice coverage and thickness continue to decrease in the Arctic, more areas of open water will exist closer to the Pole. We expect that these conditions will generate more winds due to jets such as those described here and also for other reasons such as deeper ABLs, weaker inversions, local generation of mesoscale systems such as polar lows and changes in synoptic-scale storm tracks. However, if future conditions favor more surface winds that flow along-ice edges with the ice on the left looking downwind, which is usually from the west, then the baroclinic effects of ice edge regions would slow the surface winds because the thermal wind decreases the geostrophic wind closer to the surface in these situations. Note that a northward retreat of the ice edge also suggests that winds in areas currently affected by ice-edge jets may decrease from this ice-edge effect, but may increase from other effects, such as an increased over-water fetch. The challenge for future climate predictions in the Arctic is to be able to capture important low-level effects such as the baroclinic jets described in this paper.

Acknowledgments

We thank the captain and crew of the *R/V Sikuliaq*, and all the scientists on the Sea State cruise and on shore who made this work possible. A special thanks to Chief Scientist Jim Thomson for his tireless efforts on all aspects of the Sea State program. This work was funded by the Office of Naval Research Arctic and Global Prediction Department, Code 32, managed by Scott Harper and (formerly) Martin Jeffries, grant N0001413WX20830 (Guest, Jordan), N0001417IP00027, N0001414IP20038 (Fairall),N00014-16-1-2018 (Persson, Blomquist), and under the ONR's Earth System Prediction Capability Program (Wang, Jin). None of the authors of this paper have any real or perceived financial conflicts of interest. None of the other affiliations for any author could be perceived as having a conflict of interest with respect to the results of this paper. The data used for this paper are available at http://drive.google.com/ "Collaboratory: Arctic Sea State DRI" Processed Data. Supporting information and a cruise report are at http://www.apl.uw.edu/arcticseastate.

References

Andreas, E. L., Claffey, K. J., & Makshtas, A. P. (2000). Low-level atmospheric jets and inversions over the western Weddell Sea. *Boundary-Layer Meteorology*, *97*(3), 459–486.

Blackadar, A. K. (1957). Boundary layer wind maxima and their significance for the growth of nocturnal inversions. *Bulletin of the American Meteorological Society*, *38*, 283–290.

Bintanja, R., van der Linden, E. C., & Hazeleger, W. (2012). Boundary layer stability and Arctic climate change: A feedback study using EC-Earth. *Climate Dynamics*, *39*(11), 2659. https://doi.org/10.1007/s00382-011-1272-1

Chao, S. (1985). Coastal jets in the lower atmosphere. *Journal of Physical Oceanography*, *15*, 361–371. https://doi.org/10.1175/1520-0485(1985)015 < 0361:CJITLA>2.0.CO;2

Cummings, J. A., & Smedstad, O. M. (2013). Variational data assimilation for the global ocean. In Park, S. K. & Xu, L. (Eds.), *Data assimilation for atmospheric, oceanic and hydrologic applications* (Vol. 2, pp. 303–343). Berlin, Germany: Springer-Verlag. https://doi.org/10.1007/978-3-642-35088-7

Daley, R., & Barker, E. (2001). NAVDAS: Formulation and diagnostics. *Monthly Weather Review*, *129*, 869–883.

Davidson, K. L., Boyle, P. J., & Guest, P. S. (1992). Atmospheric boundary layer properties affecting wind forecasting in gulf and coastal regions. *Journal of Applied Meteorology*, *31*, 983–994. https://doi.org/10.1175/1520-0450(1992)031

Doyle, J. D., & Warner, T. T. (1993). A three-dimensional numerical investigation of a Carolina coastal low-level jet during GALE IOP 2. *Monthly Weather Review*, *121*, 1030–1047.

Grisogono, B., Ström, L., & Tjernström, M. (1998). Small-scale variability in the coastal atmospheric boundary layer. *Boundary-Layer Meteorology*, *88*(1), 23–46. https://doi.org/10.1023/A:1000933822432

Guest, P., Glendening, J., & Davidson, K. (1995). An observational and numerical study of wind stress variations within marginal ice zones. *Journal of Geophysical Research*, *100*(C6), 10887–10904. https://doi.org/10.1029/94JC03391

Hodur, R. M. (1997). The Naval Research Laboratory's coupled ocean/atmosphere mesoscale prediction system (COAMPS). *Monthly Weather Review*, *125*, 1414–1430.

Hoerton, H., Feltham, D., & Hunt, J. (2014). The response of the sea ice edge to atmospheric and oceanic jet formation. *Journal of Physical Oceanography*, *44*, 2292–2316. https://doi.org/10.1175/JPO-D-13-0184.1

Inoue, J., Hori, M. E., Tachibana, Y., & Kikuchi, T. (2010). A polar low embedded in a blocking high over the Pacific Arctic. *Geophysical Research Letters*, *37*, L14808. https://doi.org/10.1029/2010GL043946

Jakobson, L., Vihma, T., Jakobson, E., Palo, T., Mannik, A., & Jaagus, J. (2013). Low-level jet characteristics over the Arctic Ocean in spring and summer. *Atmospheric Chemistry and Physics*, *13*, 11089–11099. https://doi.org/10.5194/acp-13-11089-2013

Langland, R., Tag, P., & Fett, R. (1989). An ice breeze mechanism for boundary-layer jets. *Boundary-Layer Meteorology*, *48*, 177–195.

Mellor, G. L., & Yamada, T. (1982). Development of a turbulence closure model for geophysical fluid problems. *Reviews of Geophysics*, *20*(4), 851–875. https://doi.org/10.1029/RG020i004p00851

Moritz, R. E. (1977). On a possible sea-breeze circulation near Barrow, Alaska. *Arctic and Alpine Research*, *9*, 427–431.

Overland, J. E., & Guest, P. S. (1991). The Arctic snow and air temperature budget over sea ice during winter. *Journal of Geophysical Research*, *96*(C3), 4651–4662. https://doi.org/10.1029/90JC02264

Persson, P. O. G., Blomquist, B., Guest, P., Stammerjohn, S., Fairall, C., Rainville, L., et al. (2018). Shipboard observations of the meteorology and near-surface environment during autumn freeze-up in the Beaufort/Chukchi Seas. *Journal of Geophysical Research: Oceans*, *123*. https://doi.org/2018JC013786

Persson, P. O. G., & Vihma, T. (2016). The atmosphere over sea ice. In Thomas, D. N. (Ed.), *Introduction to sea ice* (Chapter 6, 3rd ed.). London, UK: Wiley-Blackwell.

Price, D. (2016). *An observational and analytical study of marginal ice zone atmospheric jets* (MS thesis). Monterey, CA: Naval Postgraduate School. Retrieved from http://hdl.handle.net/10945/51598

Renfrew, I. A., & Anderson, P. S. (2006). Profiles of katabatic flow in summer and winter over Coats Land, Antarctica. *Quarterly Journal of the Royal Meteorological Society*, *132*(616), 779–802. https://doi.org/10.1256/qj.05.148

Savijärvi, H., Niemelä, S., & Tisler, P. (2005). Coastal winds and low-level jets: Simulations for sea gulfs. *Quarterly Journal of the Royal Meteorological Society*, *131*, 625–637.

Smedman, A., Tjernström, M., & Högström, U. (1993). Analysis of the turbulence structure of a marine low-level jet. *Boundary-Layer Meteorology*, *66*, 105–126. https://doi.org/10.1007/BF00705462

Smith, M., Stammerjohn, S., Persson, O., Rainville, L., Liu, G., Perrie, W., et al. (2018). Episodic reversal of the autumn ice advance caused by release of ocean heat in the Beaufort Sea. *Journal of Geophysical Research: Oceans*, *123*. https://doi.org/10.1002/2018JC013764

Spreen, G., Kaleschke, L., & Heygster, G. (2008). Sea ice remote sensing using AMSR-E 89 GHz channels. *Journal of Geophysical Research*, *113*, 2156–2202. https://doi.org/10.1029/2005JC003384

Terpstra, A., Michel, C., & Spengler, T. (2016). Forward and reverse shear environments during polar low genesis over the Northeast Atlantic. *Monthly Weather Review*, *144*, 1314–1354. https://doi.org/10.1175/MWR-D-15-0314.1

Thomson, J., Ackley, S., Girard-Ardhuin, F., Ardhuin, F., Babanin, A., Boutin, G., et al. (2018). Overview of the Arctic sea state and boundary layer physics program. *Journal of Geophysical Research*, *123*. https://doi.org/10.1002/2018JC013766

Thomson, J., Fan, J., Stammerjohn, S., Stopa, J., Rogers, W. E., Girard-Ardhuin, F., et al. (2016). Emerging trends in the sea state of the Beaufort and Chukchi Seas. *Ocean Modeling*, *105*, 1–12. https://doi.org/10.1016/j.ocemod.2016.02.009

Tuononen, M., Sinclair, V., & Vihma, T. (2015). Climatology of low-level jets in the midlatitudes and polar regions of the Northern Hemisphere. *Atmospheric Science Letters*, *16*, 492–499. https://doi.org/10.1002/asl.587

Vaisala (2013). *RS-92-SGP data sheet*. Vantaa, Finland: Vaisala. Retrieved from https://www.vaisala.com/sites/default/files/documents/RS92SGP-Datasheet-B210358EN-F-LOW.pdf

Vihma, T., & Brümmer, B. (2002). Observations and modelling of on-ice and off-ice flows in the northern Baltic Sea. *Boundary-Layer Meteorology*, *103*, 1–27.

Walter, B., & Overland, J. E. (1991). Aircraft observations of the mean and turbulent structure of the atmospheric boundary layer during spring in the central arctic. *Journal of Geophysical Research*, *96*(C3), 4663–4673. https://doi.org/10.1029/90JC02263

Wang, J., Kim, H., & Chang, E. (2017). Changes in the Northern Hemisphere winter storm tracks under the background of Arctic amplification. *Journal of Climate*, *30*(10), 3705–3724. https://doi.org/10.1175/JCLI-D-16-0650.1